

Stacked Intelligent Metasurface Assisted Multiuser Communications: From a Rate Fairness Perspective

Junjie Fang, Chao Zhang, Jiancheng An, Hongwen Yu, and Qingqing Wu, *Senior Member, IEEE*,
Mérrouane Debbah, *Fellow, IEEE*, and Chau Yuen, *Fellow, IEEE*

Abstract—Stacked intelligent metasurface (SIM) extends the concept of single-layer reconfigurable holographic surfaces (RHS) by incorporating a multi-layered structure, thereby providing enhanced control over electromagnetic wave propagation and improved signal processing capabilities. This study investigates the potential of SIM in enhancing the rate fairness in multiuser downlink systems by addressing two key optimization problems: maximizing the minimum rate (MR) and maximizing the geometric mean of rates (GMR). The former strives to enhance the minimum user rate, thereby ensuring fairness among users, while the latter relaxes fairness requirements to strike a better trade-off between user fairness and system sum-rate (SR). For the MR maximization, we adopt a consensus alternating direction method of multipliers (ADMM)-based approach, which decomposes the approximated problem into sub-problems with closed-form solutions. For GMR maximization, we develop an alternating optimization (AO)-based algorithm that also yields closed-form solutions and can be seamlessly adapted for SR maximization. Numerical results validate the effectiveness and convergence of the proposed algorithms. Comparative evaluations show that MR maximization ensures near-perfect fairness, while GMR maximization balances fairness and system SR. Furthermore, the two proposed algorithms respectively outperform existing related works in terms of MR and SR performance. Lastly, SIM with lower power consumption achieves performance comparable to that of multi-antenna digital beamforming.

Index Terms—Stacked intelligent metasurface, max-min, geometric mean, rate fairness, iterative algorithms.

I. INTRODUCTION

The sixth generation (6G) mobile communication network is envisioned to support peak data rates of up to 1 terabit per second and ultra-low latency of around 1 millisecond, driven by the demands of applications such as ultra-high-definition streaming, augmented and virtual reality (AR/VR), and the expanding Internet of Things (IoT) [1]. As massive multiple-input multiple-output (MIMO) technology can provide significant spatial diversity and enhance network capacity greatly, it has been regarded as a promising technology to

address these demands [1]. Unfortunately, it also presents challenges, including high implementation costs, substantial power consumption, and the complexity of real-time digital signal processing [2]. Hence, as data demands continue to rise, there is an urgent need for more cost-effective and energy-efficient solutions [3]. Inspired by the robust spatial multiplexing and beamforming capability brought by massive MIMO, researchers are now exploring extremely dense (and even theoretically infinite) low cost arrays to achieve even greater spatial resolution and more precise beam control [4].

Emerging from breakthroughs in metasurfaces and intelligent material design, reconfigurable intelligent surface (RIS) is perceived as a transformative technology in wireless communication systems due to a variety of fascinating features, such as low cost, low energy-consumption, low latency, high energy efficiency, and dynamic programmability [2]. Specifically, a RIS typically consists of dense arrays of sub-wavelength passive/active elements that can dynamically adjust the phases and/or amplitudes of incident electromagnetic (EM) waves, thereby achieving remarkable fine-grained beamforming gains [5]. Currently, RIS can be roughly categorized into two groups based on their function in wireless communication systems [6]. The first category, commonly referred to as intelligent reflecting surfaces (IRS), provides additional reflective links for transceivers to enhance link quality, extend coverage, and improve network capacity [7]. The second category, commonly known as reconfigurable holographic surface (RHS), is typically integrated with radio frequency (RF) circuits and serves as transceiver antenna [6]. However, recent studies have shown that existing RHS is constrained by its single-layer structure, which may limit the design degrees-of-freedom (DoF) for holographic beamforming [8]–[12].

A novel structure known as stacked intelligent metasurface (SIM) has recently gained increasing attention [10]. The pioneer work of SIM in [8] demonstrated a programmable multi-layer digital-coding metasurface array, which is proved to be suitable for signal processing in wireless systems. Further, in [10], An et al. proposed an SIM-assisted holographic MIMO framework, where an SIM consists of multiple layers of programmable metasurfaces housed in a hermetically sealed container, with sub-wavelength passive elements in each layer. The authors also affirmed that almost perfect parallel channels can be constructed between transmitter and receiver as the number of SIM layers increases. More specifically speaking, the multi-layer structure allows for finer granularity in phase and amplitude modulation and provides increased flexibility in beam pattern adjustment. To minimize processing delays

Junjie Fang and Chao Zhang are with School of Information and Communications Engineering, Xi'an Jiaotong University, Xi'an 710049, China (e-mail: fjjzcy@stu.xjtu.edu.cn, chaozhang@xjtu.edu.cn) (*Corresponding author: Chao Zhang*)

Jiancheng An and Chau Yuen are with the School of Electrical and Electronics Engineering, Nanyang Technological University, Singapore 639798 (e-mail: jiancheng_an@163.com, chau.yuen@ntu.edu.sg)

Hongwen Yu is with the School of Communication and Information Engineering, Shanghai University, Shanghai 200444, China (e-mail: hw_yu@shu.edu.cn)

Qingqing Wu is with Department of Electronic Engineering, Shanghai Jiao tong University, Shanghai 200240, China (e-mail: qingqingwu@sjtu.edu.cn).

Mérrouane Debbah is with Khalifa University of Science and Technology, P O Box 127788, Abu Dhabi, UAE (e-mail: merouane.debbah@ku.ac.ae)

TABLE I
COMPARISON OF OUR WORK WITH EXISTING SIM-RELATED EFFORTS

Literature	MIMO Setup	Objective				Method	Closed-form	Rate fairness
		MR	GMR	Sum/Achievable rate	MSINR			
[9], [13]–[15]	MU-MISO			✓		AO+PGA		
[16]	MU-MISO			✓		DRL		
[17]	Secure MU-MISO			✓		AO+PGA		
[18]	ISAC			✓		Gradient descent		
[19]	MU-MISO				✓	Gradient descent-ascent		✓
[20]	MU-MIMO			✓		MM	✓	
[21]	MU-MIMO			✓		AO+PGA		
[22]	CF-MIMO			✓		AO		
[23]	UL CF-MIMO			✓		AO	✓	
[24]	P2P MIMO			✓		PGA		
[25]	P2P MIMO			✓		AO		
This work	MU-MISO	✓	✓	✓		Consensus-ADMM+AO	✓	✓

and energy consumption associated with digital beamforming, as well as to mitigate the effects of two-hop path loss, SIM is typically integrated with transmit or/and receive antennas, which enables it to perform holographic precoding or/and combining directly in the EM wave domain [13].

Inspired by [10], SIM-enabled wireless communication systems represent an innovative concept, with a growing body of studies emerging in the current literature. In [9] and [13], based on projected gradient ascent (PGA) methods, the joint optimization algorithms of transmit power allocation at base station (BS) and wave-field beamforming at SIM were proposed to maximize the sum-rate (SR) in SIM-assisted multiuser multiple-input single-output (MU-MISO) downlink systems. With statistical channel state information (CSI), the optimal beamforming was addressed to maximize the SR by [14] in SIM-assisted MU-MISO systems. In [15], a novel low-earth orbit satellite MU-MISO communication system assisted by SIM was introduced to maximize the ergodic SR with statistical CSI. In [16], a deep reinforcement learning (DRL)-based optimization algorithm was designed to maximize the SR in MU-MISO downlink systems. In [17], a methodology was proposed to maximize the sum secrecy rate in SIM-assisted MU-MISO downlink systems. In integrated sensing and communication (ISAC) systems, the optimal beamforming was studied to maximize the SR in [18]. In [19], the minimum signal-to-interference-plus-noise ratio (MSINR) maximization problem was studied for MU-MISO downlink systems under both statistical and instantaneous CSI conditions. Besides, in [20], a dual-polarized stacked metasurface transceiver architecture was proposed in MU-MIMO systems to solve the generalized SR maximization problem. Besides, in [20], a dual-polarized stacked metasurface transceiver architecture was proposed for MU-MIMO systems, where the generalized sum-rate maximization problem was addressed using a majorization-minimization (MM)-based algorithm. In [21], a joint optimization algorithm of BS-side and channel-side SIM phase shifts was proposed to maximize the sum spectral efficiency for double-SIM-assisted MU-MIMO systems. In [22], a joint optimization algorithm was proposed to maximize the SR in SIM-assisted cell-free MIMO (CF-MIMO) systems. [23] proposed an SIM-based architecture for uplink (UL) CF-MIMO systems to enhance

achievable spectral and energy efficiency (EE). Furthermore, in [24], a beamforming optimization algorithm based on PGA methods was proposed to maximize the achievable rate in SIM-assisted Point-to-Point (P2P) MIMO systems. In [25], two optimization problems: achievable rate maximization and inter-stream interference minimization were studied in SIM-assisted P2P MIMO systems.

A. Motivation and Contributions

Current research on multiuser systems predominantly focuses on the SR maximization problem, e.g., [9], [13], [15]–[18], [20]–[22]. Although SR maximization ensures high overall throughput, it may lead to potential rate fairness issues, as users with poor channel conditions might be assigned limited or even no resources (e.g., transmit power), thereby resulting in low or zero achievable rates. This can negatively affect the overall user experience and quality of service (QoS). Although SIM has shown the substantial potential of mitigating multiuser interference [10], existing works have largely overlooked how SIM can be leveraged to improve rate fairness in multiuser systems. A recent study [19] made a valuable step in this direction by addressing rate fairness through MSINR maximization. While insightful, MSINR maximization can be viewed as a simplified surrogate of minimum rate (MR) maximization. Given that the logarithmic function in the rate expression is inherently non-linear, the solutions to the optimization problem with the multi-user rate function as the optimization objective may not be consistent with those of the optimization problem with the multi-user SINR function as the optimization objective. Our work, conducted almost concurrently with [19], provides a more comprehensive perspective by focusing directly on rate-based fairness criteria. In particular, we investigate two commonly adopted objectives: MR maximization and geometric mean of rates (GMR) maximization, which better capture fairness at the user level and offer a more balanced trade-off between fairness and SR. In our system design, SIM is integrated with the radome of the BS and performs transmit beamforming in the EM wave domain to serve multiple users simultaneously. For clarity, a preliminary categorization and comparison of related literature, is presented in Table I. Moreover, through comparative simulation experiments, we have demonstrated

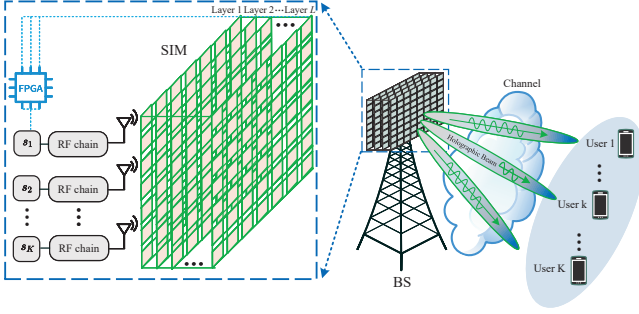


Fig. 1. An SIM-assisted multiuser wireless communication system (denote layer 1, layer 2, layer L).

that the multiuser rate performance of this work are superior to those of similar works, e.g., [9], [19].

Our main contributions can be summarized in detail as follows:

- To enhance rate fairness among users, we maximize the MR by jointly optimizing power allocation at the BS and phase shifts at the SIM. Due to the problem's non-convexity, we propose an iterative algorithm that provides closed-form solutions. Specifically, we approximate the user rate with a tractable lower bound to reformulate the problem. By leveraging the consensus alternating direction method of multipliers (ADMM) method, we decompose the original problem into several simpler sub-problems, which allows us to tailor customized optimization methods, yielding closed-form solutions.
- To balance rate fairness and SR, we formulate the GMR maximization problem. Unlike MR maximization, it combines geometric mean function and logarithmic rate function and thus lead to strong coupling among optimization variables. By exploiting the concavity of the geometric mean function and leveraging a linear approximation, we approximately decompose it into two sub-problems: power allocation at the BS and phase shift optimization at the SIM, both of which admit closed-form solutions. Besides, this algorithm can be seamlessly applied in SR maximization problem.
- Numerical results confirm the benefits of SIM deployment and validate the convergence of the proposed algorithms. A comparative analysis across multiple performance metrics, using SR maximization as a benchmark, reveals that MR maximization optimization ensures near-perfect fairness, as indicated by metrics such as MR, rate standard deviation, and min-rate/max-rate ratio. Meanwhile, GMR maximization achieves a balance between fairness and SR, positioning its performance between MR maximization and SR maximization. Besides, the proposed algorithms outperform existing methods from [9] and [19] in terms of the MR and SR, respectively. Finally, our results show that SIM attains system-limit performance comparable to multi-antenna digital beam-forming while reducing power consumption.

B. Organization and Notation

The rest of this paper is organized as follows. Section II presents system model and problem formulation. The proposed optimization algorithms for the MR maximization optimization and GMR maximization are shown in Sections III and IV, respectively. Section V evaluates the performance of the proposed algorithms. Finally, Section VI concludes the paper.

Notation: Bold upper-case and lower-case letters represent matrices and vectors, respectively, while italic letters denote scalars. $(\cdot)^T$, $(\cdot)^*$, and $(\cdot)^H$ represent transpose, conjugate, and conjugate transpose, respectively. \odot denotes the Hadamard product. The real part of (\cdot) is denoted by $\Re(\cdot)$. $\arg(\cdot)$ denotes the phase information of (\cdot) . For a complex vector \mathbf{x} , $\text{diag}(\mathbf{x})$ represents a diagonal matrix whose diagonal entries are composed of elements of \mathbf{x} and $[\mathbf{x}]_m$ denote the m -th element of \mathbf{x} . For a square matrix \mathbf{X} , $\text{Tr}(\mathbf{X})$, \mathbf{X}^{-1} , $|\mathbf{X}|$, and $[\mathbf{X}]_{a,b}$ denote its trace, inverse, determinant, and the element in the a -th row and b -th column.

II. SYSTEM MODEL AND PROBLEM FORMULATION

A. System Model

We consider a multiuser MISO downlink wireless communication system assisted by an SIM, as shown in Fig. 1. In this system, a BS with M antennas transmits signals to K single-antenna users. The SIM comprises L layers of stacked reconfigurable metasurfaces, which are uniformly managed by an intelligent controller, and each layer consists of N meta-atoms. To avoid performance degradation caused by two-hop path loss and reduce the transmission burden of real-time information exchanges, the SIM is integrated with the antenna radome of the BS [13]. Additionally, to prevent interference from undesired diffraction, scattering, and ambient noise, the components are encapsulated within a sealed vessel [10]. Specifically, the EM wave emitted by the BS passes through each layer of the SIM in sequence, with each layer using a controller to adjust the characteristics of the incident EM wave, such as its phase and/or amplitude, to precisely manipulate the wavefront and achieve multiuser precoding automatically for enhancing overall transmission performance [11].

We define the set of transmit antennas, SIM layers, all elements on each metasurface layer, and users by $\mathcal{M} = \{1, 2, \dots, M\}$, $\mathcal{L} = \{1, 2, \dots, L\}$, $\mathcal{N} = \{1, 2, \dots, N\}$, and $\mathcal{K} = \{1, 2, \dots, K\}$, respectively. Taking into account the balance between energy efficiency and implementation costs, we solely focus on the phase-shifting capability of these elements, as [13], [15]–[18], [20]–[22]. Hence, we assume that the amplitude coefficients of all elements are set to unit. Then, we define the coefficient vector of the l -th layer of the SIM as $\mathbf{e}^{j\theta_l} = [e^{j\theta_{l,1}}, e^{j\theta_{l,2}}, \dots, e^{j\theta_{l,N}}]$, where $\theta_{l,n} \in [0, 2\pi)$ is the phase shift of the n -th meta-atom on the l -th metasurface layer, for $n \in \mathcal{N}$ and $l \in \mathcal{L}$. And then we can define $\Theta_l = \text{diag}(\mathbf{e}^{j\theta_l})$. Let $\mathbf{W}_l \in \mathbb{C}^{N \times N}$, for $l \in \mathcal{L}$, $l \neq 1$, and $\mathbf{W}_1 = [\mathbf{w}_{1,1}, \mathbf{w}_{1,2}, \dots, \mathbf{w}_{1,M}] \in \mathbb{C}^{N \times M}$ denote the channel response matrix from the $(l-1)$ -th metasurface layer to the l -th metasurface layer, and the channel response matrix from the BS to the 1-th metasurface layer, respectively. For $k \in \mathcal{K}$, $\mathbf{h}_{\text{SIM}-k}^H \in \mathbb{C}^{1 \times N}$ stands for the channel vector from the

SIM to the k -th user. According to the Rayleigh-Sommerfeld diffraction theory, the element of the channel response matrix \mathbf{W}_l in the n -th row and n' -th column, for $n, n' \in \mathcal{N}$, $l \in \mathcal{L}$, $l \neq 1$, is given by [9]–[12]

$$[\mathbf{W}_l]_{n,n'} = \frac{d_l d_w d_t}{(L-1)d_{n,n'}^2} \left(\frac{1}{2\pi d_{n,n'}} - \frac{j}{\lambda_c} \right) e^{\frac{j2\pi d_{n,n'}}{\lambda_c}}, \quad (1)$$

where d_l and d_w represent the length and width of the SIM meta-atoms, d_t denotes the thickness of the whole SIM, $d_{n,n'}$ is the distance between the n -th meta-atom on the l -th layer and the n' -th meta-atom on the $(l-1)$ -th layer, and λ_c denotes the carrier wavelength. Since the SIM is mounted on the BS, the transmission from BS to SIM falls within the near-field line-of-sight (LoS) regime. Based on the spherical wave propagation characteristics, the meta-atom of the channel response matrix \mathbf{W}_1 in the n -th row and m -th column, for $n \in \mathcal{N}$, $m \in \mathcal{M}$, is given by [9]–[12]

$$[\mathbf{W}_1]_{n,m} = \frac{\lambda_c}{4\pi d_{n,m}} e^{\frac{-j2\pi d_{n,m}}{\lambda_c}}, \quad (2)$$

where $d_{n,m}$ is the distance between the n -th meta-atom on the 1st layer and the m -th antenna of the BS. Then, the equivalent EM wave domain beamforming matrix of the SIM can be given by

$$\mathbf{G} = \mathbf{\Theta}_L \mathbf{W}_L \mathbf{\Theta}_{L-1} \mathbf{W}_{L-1} \cdots \mathbf{\Theta}_2 \mathbf{W}_2 \mathbf{\Theta}_1 \in \mathbb{C}^{N \times N}. \quad (3)$$

To focus solely on the wave-based beamforming gain enabled by the SIM and avoid the complications of antenna selection, we assume $K = M$, as in [9]–[12], [15], [23], [24]. This simplification removes the need to pre-select K transmit antennas from M candidates, which is a typical challenge in conventional MIMO systems with limited RF chains. The joint design of antenna selection and SIM-based beamforming is left for future work. Specifically, each antenna at the BS just transmits a signal intended for one user, while the BS focuses solely on power allocation, without participating in digital beamforming design. Additionally, we assume knowledge of the instantaneous CSI for all channels, which can be obtained by leveraging advanced channel estimation methods proposed in [26], [27]. It is worth noting that the algorithms presented in this paper can be easily adapted, with minor modifications, to scenarios where both the BS and SIM participate in beamforming design.

Consequently, for $k \in \mathcal{K}$, the received signal at the k -th user can be expressed as

$$y_k = \mathbf{h}_{\text{SIM-}k}^H \mathbf{G} \mathbf{W}_1 \mathbf{x} + n_k, \quad (4)$$

where $\mathbf{x} = [\sqrt{p_1}s_1, \sqrt{p_2}s_2, \dots, \sqrt{p_K}s_K] \in \mathbb{C}^{M \times 1}$, p_k denotes the BS transmit power allocated to the k -th user, s_k is the desired signal for the k -th user and follows the Gaussian distribution with zero mean and unit variance, i.e., $s_k \sim \mathcal{CN}(0, 1)$, and $n_k \sim \mathcal{CN}(0, \sigma_k^2)$ is the independent and identically distributed (i.i.d.) Gaussian noise. The received SINR at the k -th user is given by

$$\text{SINR}_k = \frac{|\mathbf{h}_{\text{SIM-}k}^H \mathbf{G} \mathbf{w}_{1,k}|^2 p_k}{\sum_{m=1, m \neq k}^K |\mathbf{h}_{\text{SIM-}k}^H \mathbf{G} \mathbf{w}_{1,m}|^2 p_m + \sigma_k^2}. \quad (5)$$

Then, the achievable rate of the k -th user can be expressed by

$$r_k = \log_2(1 + \text{SINR}_k). \quad (6)$$

It is worth highlighting that existing research predominantly emphasizes SR maximization, typically compromising user fairness, which underscores the motivation for our study.

B. Problem Formulation

In this work, we focus on two commonly encountered rate fairness optimization problems: the MR maximization and the GMR maximization, to equitably evaluate the effect of SIM on enhancing rate fairness.

1) *MR Maximization*: The goal here is to maximize the minimum achievable rate across all K users, i.e., $\max\{\min r_k\}$ for $k \in \mathcal{K}$, by jointly optimizing the power allocation coefficients $\{p_k\}$ at the BS and the beamforming matrices $\{\mathbf{\Theta}_l\}$ for $l \in \mathcal{L}$ at the SIM, with the total power constraint at the BS and the transmission coefficient constraints at the SIM. To facilitate the optimization problem, we define the auxiliary variable $\rho_k = \sqrt{p_k}$ for $k \in \mathcal{K}$. Mathematically, the MR maximization problem can be expressed as

$$(\text{P1}) : \max_{\{\rho_k, \mathbf{\Theta}_l\}, \gamma} \gamma \quad (7)$$

$$\text{s.t. } r_k \geq \gamma, k \in \mathcal{K}, \quad (7a)$$

$$\sum_{k=1}^K \rho_k^2 \leq P_{\max}, \quad (7b)$$

$$\rho_k \geq 0, k \in \mathcal{K}, \quad (7c)$$

$$0 \leq \theta_{l,n} \leq 2\pi, n \in \mathcal{N}, l \in \mathcal{L}. \quad (7d)$$

where P_{\max} is the maximum allowable total transmit power at the BS. From (P1), we can see that rates of all users are always larger than γ , which represents the required minimum QoS for all users. Thus, the rates of the users experiencing poor channel conditions are also guaranteed, rather than being forced to be few or even zero in SR optimization. As a result, in the MR maximization framework, the rate fairness of all users is improved to a certain extent.

2) *GMR Maximization*: Clearly, MR maximization may not fully leverage the system's potential for maximizing overall SR. In contrast, the second problem, GMR maximization, aims to balance individual users' rates by promoting a more equitable distribution, potentially improving overall system performance without disproportionately benefiting any single user. With the same constraints at the BS and SIM, the GMR maximization problem can be formulated as

$$(\text{P2}) : \max_{\{\rho_k, \mathbf{\Theta}_l\}} \left(\prod_{k=1}^K r_k \right)^{1/K} \quad (8)$$

$$\text{s.t. } (7b), (7c), (7d). \quad (8a)$$

Although GMR maximization may not always try to promote the rate for the most disadvantaged user, in [28] it is shown that maximizing the GMR can achieve Pareto-optimal rates, therefore ensuring a degree of rate fairness along with favorable SINR. Moreover, the GMR maximization problem is computationally simpler due to the absence of the mandatory

and intractable constraint (7a) found in (P1), leading to a relatively lower algorithmic complexity.

We can see that both (P1) and (P2) are highly non-convex, as (P1) has its non-convex constraint (7a) and the objective function of (P2) is non-concave. And especially when L and N become very large, both problems would result in a more intricate optimization landscape, due to a high prevalence of local optima and saddle points in solving process. Therefore, the development of efficient algorithms is extremely crucial to advance the practical applications of SIM. Next, we separately design solving algorithms for above two problems.

III. SOLVING ALGORITHM FOR MR MAXIMIZATION

A. MR Maximization Algorithm Design

The existence of the auxiliary variable γ in (7a) forces us to directly deal with r_k in order to avoid the intricate coupling between $\{\rho_k, \Theta_l\}$ and γ . Therefore, given a feasible solution, we intend to develop a feasible lower bound for r_k to construct the approximate optimization problem of (P1) [29]–[31].

It is noted that r_k is not jointly concave with respect to (w.r.t.) $\{\rho_k\}$ and $\{\Theta_l\}$. For convenience, i.e., to avoid dealing with the intricate coupling between $\{\rho_k\}$ and $\{\Theta_l\}$ in r_k of (7a), we first integrate $\{\rho_k\}$ and $\{\Theta_l\}$ into an auxiliary variable $\{\mathbf{A}_k\}$. According to the partitioned matrix inversion lemma, r_k in (6) is equivalent to

$$r_k = \log_2 (\mathbf{p} \mathbf{A}_k^{-1} \mathbf{p}^T), \quad (9)$$

where

$$\mathbf{p} = [1, 0],$$

$$\mathbf{A}_k = \begin{bmatrix} 1 & (\mathbf{h}_{\text{SIM}-k}^H \mathbf{G} \mathbf{w}_{1,k} \rho_k)^H \\ \mathbf{h}_{\text{SIM}-k}^H \mathbf{G} \mathbf{w}_{1,k} \rho_k & \sum_{m=1}^K |\mathbf{h}_{\text{SIM}-k}^H \mathbf{G} \mathbf{w}_{1,m} \rho_m|^2 + \sigma_k^2 \end{bmatrix} \in \mathbb{C}^{2 \times 2}.$$

We can find that r_k in (9) is convex w.r.t. \mathbf{A}_k . Accordingly, due to the first-order property of convex function, we can derive the lower bound of r_k given a certain feasible solution. Assuming that $\{\rho_k^{(i)}\}$ and $\{\Theta_l^{(i)}\}$ are arbitrary feasible solutions obtained in the i -th round, we can then obtain the corresponding $\mathbf{G}^{(i)}$, $\mathbf{A}_k^{(i)}$, and $\text{SINR}_k^{(i)}$. Consequently, the lower bound of r_k in the $(i+1)$ -th round can be expressed as

$$\hat{r}_{k,i} \triangleq \frac{1}{\ln 2} \left(c_k^{(i)} - 2\Re \left(b_{k,12}^{(i)} \mathbf{h}_{\text{SIM}-k}^H \mathbf{G} \mathbf{w}_{1,k}^1 \rho_k \right) - b_{k,22}^{(i)} \sum_{m=1}^K |\mathbf{h}_{\text{SIM}-k}^H \mathbf{G} \mathbf{w}_{1,m}^1 \rho_m|^2 \right) \leq r_k, \quad (10)$$

where

$$c_k^{(i)} = \ln (\mathbf{p} (\mathbf{A}_k^{(i)})^{-1} \mathbf{p}^T) + \text{Tr} (\mathbf{B}_k^{(i)} \mathbf{A}_k^{(i)}) - b_{k,11}^{(i)} - \sigma_k^2 b_{k,22}^{(i)},$$

$$\mathbf{B}_k^{(i)} = (\mathbf{A}_k^{(i)})^{-1} \mathbf{p}^T \left(\mathbf{p} (\mathbf{A}_k^{(i)})^{-1} \mathbf{p}^T \right)^{-1} \mathbf{p} (\mathbf{A}_k^{(i)})^{-1},$$

and $b_{k,uv}^{(i)}$ for $u, v \in \{1, 2\}$ are sub-blocks of $\mathbf{B}_k^{(i)}$, i.e.,

$$\mathbf{B}_k^{(i)} = \begin{bmatrix} b_{k,11}^{(i)} & b_{k,12}^{(i)} \\ b_{k,21}^{(i)} & b_{k,22}^{(i)} \end{bmatrix}.$$

In particular, we have

$$b_{k,11}^{(i)} = 1 + \text{SINR}_k^{(i)}, \quad (11)$$

$$b_{k,12}^{(i)} = \left(b_{k,21}^{(i)} \right)^* = -\text{SINR}_k^{(i)} / \mathbf{h}_{\text{SIM}-k}^H \mathbf{G}^{(i)} \mathbf{w}_{1,k} \rho_k^{(i)}, \quad (12)$$

$$b_{k,22}^{(i)} = b_{k,12}^{(i)} b_{k,21}^{(i)} / b_{k,11}^{(i)}. \quad (13)$$

Then, given $\{\rho_k^{(i)}\}$ and $\{\Theta_l^{(i)}\}$, we can get the next feasible solutions $\{\rho_k^{(i+1)}\}$ and $\{\Theta_l^{(i+1)}\}$ by solving

$$(\text{P1.1}) : \{\rho_k^{(i+1)}, \Theta_l^{(i+1)}\} = \arg \max_{\{\rho_k, \Theta_l\}, \gamma} \gamma \quad (14)$$

$$\text{s.t. } \hat{r}_{k,i} \geq \gamma, k \in \mathcal{K}, (7b), (7c), (7d). \quad (14a)$$

Unfortunately, the optimization problem (P1.1) still cannot be solved directly due to the coupling between $\{\rho_k\}$ and $\{\Theta_l\}$ in the expression of $\hat{r}_{k,i}$, e.g., (10). Since consensus-ADMM excels in solving large-scale and distributed optimization problems by decomposing an original problem into smaller, more manageable sub-problems that can be solved in parallel [32], [33], we develop a consensus-ADMM-based algorithm to solve (P1.1). One can observe that γ , $\{\rho_k\}$, and $\{\Theta_l\}$ appear in all K rate constraints in (14a), so we have to introduce auxiliary variables $z_{km} = \mathbf{h}_{\text{SIM}-k}^H \mathbf{G} \mathbf{w}_{1,m} \rho_m$ and $\eta_k = \gamma$ for $k, m \in \mathcal{K}$ to transform (P1.1) into a decomposable structure. Then, (P1.1) can be equivalently given by

$$(\text{P1.2}) : \max_{\{z_{km}, \eta_k, \rho_k, \Theta_l\}, \gamma} \gamma \quad (15)$$

$$\text{s.t. } c_k^{(i)} - 2\Re \left(b_{k,12}^{(i)} z_{kk} \right) - \sum_{m=1}^K b_{k,22}^{(i)} z_{km} z_{km}^* \geq \ln 2 \eta_k, k \in \mathcal{K}, \quad (15a)$$

$$z_{km} = \mathbf{h}_{\text{SIM}-k}^H \mathbf{G} \mathbf{w}_{1,m} \rho_m, k, m \in \mathcal{K}, \quad (15b)$$

$$\eta_k = \gamma, k \in \mathcal{K}, \quad (15c)$$

$$(7b), (7c), (7d). \quad (15d)$$

Let $\mathcal{F}_{z,\eta}$, \mathcal{F}_ρ , and \mathcal{F}_θ represent the feasible sets of variables $\{z_{km}, \eta_k\}$, $\{\rho_k\}$, and $\{\Theta_l\}$ satisfying the inequality constraints (15a), (7b), (7c), and (7d), respectively. Then, the indicator functions corresponding to $\mathcal{F}_{z,\eta}$, \mathcal{F}_ρ , and \mathcal{F}_θ can be defined by

$$\mathbb{I}_{\mathcal{F}_{z,\eta}} (\{z_{km}, \eta_k\}) = \begin{cases} 0, & \text{if } \{z_{km}, \eta_k\} \in \mathcal{F}_{z,\eta}, \\ -\infty, & \text{otherwise.} \end{cases}$$

$$\mathbb{I}_{\mathcal{F}_\rho} (\{\rho_k\}) = \begin{cases} 0, & \text{if } \{\rho_k\} \in \mathcal{F}_\rho, \\ -\infty, & \text{otherwise.} \end{cases} \quad (16)$$

$$\mathbb{I}_{\mathcal{F}_\theta} (\{\Theta_l\}) = \begin{cases} 0, & \text{if } \{\Theta_l\} \in \mathcal{F}_\theta, \\ -\infty, & \text{otherwise.} \end{cases}$$

Integrating the inequality constraints into the objective function via (16), (P1.2) can be equivalently transformed to the following consensus equality-constrained problem

$$(\text{P1.3}) : \max_{\{z_{km}, \eta_k, \rho_k, \Theta_l\}, \gamma} \mathbb{I}_{\mathcal{F}_{z,\eta}} (\{z_{km}, \eta_k\}) + \mathbb{I}_{\mathcal{F}_\rho} (\{\rho_k\}) + \mathbb{I}_{\mathcal{F}_\theta} (\{\Theta_l\}) + \gamma \quad (17)$$

$$\text{s.t. } (15b), (15c). \quad (17a)$$

According to coupling relationship introduced by constraints, the optimization variables can be split into four separate variable blocks, i.e., $\{z_{km}, \eta_k\}$, $\{\rho_k\}$, $\{\Theta_l\}$, and γ . Therefore, the augmented Lagrangian of (P1.3) is given by

$$\begin{aligned} \mathcal{L}_{P1.3}(\{z_{km}, \eta_k, \rho_k, \Theta_l, z_{d,km}, \eta_{d,k}\}, \gamma) = & \mathbb{I}_{\mathcal{F}_{z,\eta}}(\{z_{km}, \eta_k\}) + \mathbb{I}_{\mathcal{F}_\rho}(\{\rho_k\}) + \mathbb{I}_{\mathcal{F}_\Theta}(\{\Theta_l\}) + \gamma - \\ & \frac{\rho}{2} \sum_{k=1}^K \sum_{m=1}^K |z_{km} - \mathbf{h}_{\text{SIM-}k}^H \mathbf{G} \mathbf{w}_{1,m} \rho_m + z_{d,km}|^2 - \\ & \frac{\rho}{2} \sum_{k=1}^K (\eta_k - \gamma + \eta_{d,k})^2, \end{aligned} \quad (18)$$

where $\rho > 0$ denotes the penalty parameter for step-size control, $z_{d,km}$ and $\eta_{d,k}$, for $k, m \in \mathcal{K}$, are scaled dual variables associated with constraint (15b) and (15c). That is to say now we can maximize $\mathcal{L}_{P1.3}(\{z_{km}, \eta_k, \rho_k, \Theta_l, z_{d,km}, \eta_{d,k}\}, \gamma)$ w.r.t. $\{z_{km}, \eta_k\}$, $\{\rho_k\}$, $\{\Theta_l\}$, and γ to find the solution of (P1.3).

To solve (P1.3), we need to alternately update the four variable blocks and the dual variables $\{z_{d,km}, \eta_{d,k}\}$ in each round of iteration. Let $\{z_{km}^{(j)}, \eta_k^{(j)}\}$, $\{\rho_k^{(j)}\}$, $\{\Theta_l^{(j)}\}$, $\gamma^{(j)}$, and $\{z_{d,km}^{(j)}, \eta_{d,k}^{(j)}\}$ be the solutions after the j -th consensus-ADMM iteration procedure of (P1.3). Assuming that j^* is the number of consensus-ADMM iterations required to solve (P1.3), we have $\rho_k^{(i+1)} = \rho_k^{(j^*)}$, $\Theta_l^{(i+1)} = \Theta_l^{(j^*)}$, for $k \in \mathcal{K}, l \in \mathcal{L}$, which can be used to generate $\hat{r}_{k,i+1}$ and then update optimization problem (P1.2). To summarize, the whole algorithm consists of two layers of iterations, the outer iteration is used to update (P1.2) and the inner consensus-ADMM iteration is used to solve (P1.3). We next show the details of the five steps in the $(j+1)$ -th inner consensus-ADMM iteration.

STEP 1: Updating $\{z_{km}^{(j+1)}, \eta_k^{(j+1)}\}$

From (18), given $\{z_{km}^{(j)}, \eta_k^{(j)}\}$, $\{\rho_k^{(j)}\}$, $\{\Theta_l^{(j)}\}$, $\gamma^{(j)}$, and $\{z_{d,km}^{(j)}, \eta_{d,k}^{(j)}\}$, we can update $\{z_{km}, \eta_k\}$ by solving

$$\begin{aligned} \{z_{km}^{(j+1)}, \eta_k^{(j+1)}\} = \arg \max_{\{z_{km}, \eta_k\}} \mathcal{L}_{P1.3}(\{z_{km}, \eta_k, \rho_k^{(j)}, \\ \Theta_l^{(j)}, z_{d,km}^{(j)}, \eta_{d,k}^{(j)}\}, \gamma^{(j)}). \end{aligned} \quad (19)$$

By omitting the irrelevant terms $\mathbb{I}_{\mathcal{F}_\rho}(\{\rho_k^{(j)}\})$, $\mathbb{I}_{\mathcal{F}_\Theta}(\{\Theta_l^{(j)}\})$, and $\gamma^{(j)}$ in (18), (19) is equivalent to

$$\begin{aligned} \text{(P1.3.1): } \min_{\{z_{km}, \eta_k\}} \sum_{k=1}^K \left(\sum_{m=1}^K |z_{km} - \mathbf{h}_{\text{SIM-}k}^H \mathbf{G}^{(j)} \mathbf{w}_{1,m} \rho_m^{(j)} + z_{d,km}^{(j)}|^2 \right. \\ \left. + (\eta_k - \gamma^{(j)} + \eta_{d,k}^{(j)})^2 \right) \quad \text{s.t.} \quad (15a). \end{aligned} \quad (20)$$

It can be found that for $k, m \in \mathcal{K}$, z_{km} and η_k are decoupled in both objective function and constraint (15a). Therefore, (P1.3.1) can be decomposed into K convex independent quadratically constrained quadratic programming with only one constraint (QCQP-1), which can be directly solved in closed-form. Define the dual variable associated with the k -th constraint of (15a) by $\lambda_k \geq 0$. The Lagrangian w.r.t.

TABLE II
VALUES OF $z_{km}^{(j+1)}$ AND $\eta_k^{(j+1)}$

$f_{k,\lambda} \geq 0$	$z_{km}^{(j+1)} = \mathbf{h}_{\text{SIM-}k}^H \mathbf{G}^{(j)} \mathbf{w}_{1,m} \rho_m^{(j)} - z_{d,km}^{(j)}$
	$\eta_k^{(j+1)} = \gamma^{(j)} - \eta_{d,k}^{(j)}$
$f_{k,\lambda} < 0$	$z_{km}^{(j+1)} = \begin{cases} \frac{\mathbf{h}_{\text{SIM-}k}^H \mathbf{G}^{(j)} \mathbf{w}_{1,m} \rho_m^{(j)} - z_{d,km}^{(j)} - (\lambda_k b_{k,12}^{(i)})^*}{1 + \lambda_k b_{k,22}^{(i)}}, & \text{if } k = m, \\ \frac{\mathbf{h}_{\text{SIM-}k}^H \mathbf{G}^{(j)} \mathbf{w}_{1,m} \rho_m^{(j)} - z_{d,km}^{(j)}}{1 + \lambda_k b_{k,22}^{(i)}}, & \text{if } k \neq m. \end{cases}$
	$\eta_k^{(j+1)} = \gamma^{(j)} - \eta_{d,k}^{(j)} - \ln 2 \lambda_k / 2$

$\{z_{km}\}$, η_k , λ_k , for $m \in \mathcal{K}$, of the k -th sub-problem is given by

$$\begin{aligned} \mathcal{L}_{k,P1.3.1}(\{z_{km}\}, \eta_k, \lambda_k) = & \sum_{m=1}^K |z_{km} - \mathbf{h}_{\text{SIM-}k}^H \mathbf{G}^{(j)} \mathbf{w}_{1,m} \rho_m^{(j)} + z_{d,km}^{(j)}|^2 + (\eta_k - \gamma^{(j)} + \eta_{d,k}^{(j)})^2 \\ & + \lambda_k \left(\ln 2 \eta_k + 2 \Re(b_{k,12}^{(i)} z_{kk}) + \sum_{m=1}^K b_{k,22}^{(i)} z_{km} z_{km}^* - c_k^{(i)} \right). \end{aligned} \quad (21)$$

By applying the Karush-Kuhn-Tucker (KKT) condition, we can obtain $\{z_{km}^{(j+1)}, \eta_k^{(j+1)}\}$ as demonstrated in Table II by letting the gradient of $\mathcal{L}_{k,P1.3.1}(\{z_{km}\}, \eta_k, \lambda_k)$ w.r.t. z_{km} and η_k be zero, where

$$\begin{aligned} f_{k,\lambda} = c_k^{(i)} - 2 \Re(b_{k,12}^{(i)} (\mathbf{h}_{\text{SIM-}k}^H \mathbf{G}^{(j)} \mathbf{w}_{1,k} \rho_k^{(j)} - z_{d,kk}^{(j)})) - \\ b_{k,22}^{(i)} \sum_{m=1}^K |\mathbf{h}_{\text{SIM-}k}^H \mathbf{G}^{(j)} \mathbf{w}_{1,m} \rho_m^{(j)} - z_{d,km}^{(j)}|^2 - \ln 2 (\gamma^{(j)} - \eta_{d,k}^{(j)}). \end{aligned}$$

With the complementary slackness condition, there is $\lambda_k = 0$ if $f_{k,\lambda} \geq 0$. While, if $f_{k,\lambda} < 0$, $z_{km}^{(j+1)}$ and $\eta_k^{(j+1)}$ are both monotonically decreasing w.r.t. λ_k . In this case, λ_k can be effectively found by bisection searching.

STEP 2: Updating $\{\rho_k^{(j+1)}\}$:

Given $\{z_{km}^{(j+1)}, \eta_k^{(j+1)}\}$, $\{\rho_k^{(j)}\}$, $\{\Theta_l^{(j)}\}$, $\gamma^{(j)}$, and $\{z_{d,km}^{(j)}, \eta_{d,k}^{(j)}\}$, similarly we can update $\{\rho_k\}$ by solving

$$\begin{aligned} \{\rho_k^{(j+1)}\} = \arg \max_{\{\rho_k\}} \mathcal{L}_{P1.3}(\{z_{km}^{(j+1)}, \eta_k^{(j+1)}, \rho_k, \\ \Theta_l^{(j)}, z_{d,km}^{(j)}, \eta_{d,k}^{(j)}\}, \gamma^{(j)}), \end{aligned} \quad (22)$$

which is equivalent to

$$\text{(P1.3.2): } \min_{\{\rho_k\}} \sum_{k=1}^K \sum_{m=1}^K |z_{km}^{(j+1)} - \mathbf{h}_{\text{SIM-}k}^H \mathbf{G}^{(j)} \mathbf{w}_{1,m} \rho_m + z_{d,km}^{(j)}|^2 \quad \text{s.t.} \quad (7b), (7c). \quad (23a)$$

Note that (P1.3.2) becomes a convex QCQP-1 and can be solved using the similar approach for (P1.3.1). Then, $\rho_k^{(j+1)}$ can be given by

$$\rho_k^{(j+1)} = \begin{cases} \max\{0, f_{k,\beta}(0)\}, & \text{if } \sum_{k=1}^K (f_{k,\beta}(0))^2 \leq P_{\max}, \\ \max\{0, f_{k,\beta}(\hat{\beta})\}, & \text{otherwise,} \end{cases} \quad (24)$$

where

$$f_{k,\beta}(\beta) = \frac{\sum_{m=1}^K \Re\left(\left(\mathbf{h}_{\text{SIM-}m}^H \mathbf{G}^{(j)} \mathbf{w}_{1,k}\right)^* \left(z_{mk}^{(j+1)} + z_{d,mk}^{(j)}\right)\right)}{\sum_{m=1}^K \left|\mathbf{h}_{\text{SIM-}m}^H \mathbf{G}^{(j)} \mathbf{w}_{1,k}\right|^2 + \beta},$$

and $\hat{\beta} > 0$ is the optimal dual variable associated with the transmit power constraint (7b) when $\sum_{k=1}^K (f_{k,\beta}(0))^2 > P_{\max}$. Numerical evaluations confirm that $\rho_k^{(j+1)}$ consistently takes non-negative values in representative scenarios.

STEP 3: Updating $\{\Theta_l^{(j+1)}\}$:

Given $\{z_{km}^{(j+1)}, \eta_k^{(j+1)}\}$, $\{\rho_k^{(j+1)}\}$, $\{\Theta_l^{(j)}\}$, $\gamma^{(j)}$, and $\{z_{d,km}^{(j)}, \eta_{d,k}^{(j)}\}$, $\{\Theta_l\}$ can be updated by solving

$$\begin{aligned} \{\Theta_l^{(j+1)}\} &= \arg \max_{\{\Theta_l\}} \mathcal{L}_{P1.3} \left(\{z_{km}^{(j+1)}, \eta_k^{(j+1)}, \rho_k^{(j+1)}\}, \right. \\ &\quad \left. \Theta_l, z_{d,km}^{(j)}, \eta_{d,k}^{(j)}, \gamma^{(j)} \right). \end{aligned} \quad (25)$$

Also, (25) is equivalent to

$$(P1.3.3): \min_{\{\Theta_l\}} \sum_{k=1}^K \sum_{m=1}^K \left| z_{km}^{(j+1)} - \mathbf{h}_{\text{SIM-}k}^H \mathbf{G} \mathbf{w}_{1,m} \rho_m^{(j+1)} + z_{d,km}^{(j)} \right|^2 \quad (26)$$

$$\text{s.t. } 0 \leq \theta_{l,n} \leq 2\pi, n \in \mathcal{N}, l \in \mathcal{L}. \quad (26a)$$

The most significant challenge in (P1.3.3) lies in the complex coupling between phase shifts on multiple layer metasurfaces. Nevertheless, the phase shifts of all elements are completely separate in the constraint (7d). The fact inspires us to adopt the BCD method to update phase shifts alternately. Specifically, aiming at the phase shift of the n -th meta-atom on the l -th metasurface layer $\theta_{l,n}$, given $\{\theta_{l',m}\}$ and $\{\theta_{l,n'}\}$ for $l' \in \mathcal{L}, m \in \mathcal{N}$ and $n' \neq n, n' \in \mathcal{N}$, i.e., given all phase shifts except $\theta_{l,n}$, we can update $\theta_{l,n}$ by solving

$$(P1.3.3_{l,n}): \min_{\theta_{l,n}} -2\Re\left(t_{l,n}^{(j)} e^{j\theta_{l,n}}\right) + d_{l,n}^{(j)} \quad (27)$$

$$\text{s.t. } 0 \leq \theta_{l,n} \leq 2\pi, \quad (27a)$$

where

$$\begin{aligned} t_{l,n}^{(j)} &= \left[\sum_{k=1}^K \sum_{m=1}^K \mathbf{t}_{1,l,k,m}^{(j)} \right] - \sum_{n' \neq n}^N e^{-j\theta_{l,n'}} \left[\sum_{k=1}^K \sum_{m=1}^K \mathbf{T}_{2,l,k,m}^{(j)} \right]_{n',n}, \\ \mathbf{t}_{1,l,k,m}^{(j)} &= \left(\left(z_{km}^{(j+1)} + z_{d,km}^{(j)} \right) \mathbf{h}_{\text{SIM-}k}^H \mathbf{U}_l^{(j)} \right) \odot \left(\mathbf{V}_l^{(j)} \mathbf{w}_{1,m} \rho_m^{(j+1)} \right)^T, \\ \mathbf{T}_{2,l,k,m}^{(j)} &= \left(\mathbf{t}_{2,l,k,m}^{(j)} \left(\mathbf{t}_{2,l,k,m}^{(j)} \right)^H \right)^T, \\ \mathbf{t}_{2,l,k,m}^{(j)} &= \text{diag} \left(\mathbf{h}_{\text{SIM-}k}^H \mathbf{U}_l^{(j)} \right) \mathbf{V}_l^{(j)} \mathbf{w}_{1,m} \rho_m^{(j+1)}, \\ \mathbf{U}_l^{(j)} &= \Theta_L^{(j)} \mathbf{W}_L \cdots \Theta_{l+1}^{(j)} \mathbf{W}_{l+1}, \\ \mathbf{V}_l^{(j)} &= \mathbf{W}_l \Theta_{l-1}^{(j)} \mathbf{W}_{l-1} \cdots \Theta_2^{(j)} \mathbf{W}_2 \Theta_1^{(j)}, \\ d_{l,n}^{(j)} &= \sum_{k=1}^K \sum_{m=1}^K \left| z_{km}^{(j+1)} + z_{d,km}^{(j)} \right|^2 - 2\Re \left(\sum_{m \neq n}^N e^{j\theta_{l,m}} t_{l,m}^{(j)} \right). \end{aligned}$$

We can see that $d_{l,n}^{(j)}$ keep constant and $\Re\left(t_{l,n}^{(j)} e^{j\theta_{l,n}}\right) = \left| t_{l,n}^{(j)} \right| \cos\left(\arg\left(t_{l,n}^{(j)}\right) + \theta_{l,n}\right)$. Consequently, the optimal $\theta_{l,n}^{(j+1)}$ for (P1.3.3 $_{l,n}$) is given by

$$\theta_{l,n}^{(j+1)} = -\arg\left(t_{l,n}^{(j)}\right). \quad (28)$$

Based on (28), we can update all LN phase shifts alternately and thereby can obtain $\{\Theta_l^{(j+1)}\}$ and $\mathbf{G}^{(j+1)}$.

STEP 4: Updating $\gamma^{(j+1)}$:

Given $\{z_{km}^{(j+1)}, \eta_k^{(j+1)}\}$, $\{\rho_k^{(j+1)}\}$, $\{\Theta_l^{(j+1)}\}$, and $\{z_{d,km}^{(j)}, \eta_{d,k}^{(j)}\}$, γ can be updated by solving

$$\begin{aligned} \gamma^{(j+1)} &= \arg \max_{\gamma} \mathcal{L}_{P1.3} \left(\{z_{km}^{(j+1)}, \eta_k^{(j+1)}, \rho_k^{(j+1)}\}, \right. \\ &\quad \left. \Theta_l^{(j+1)}, z_{d,km}^{(j)}, \eta_{d,k}^{(j)} \right), \end{aligned} \quad (29)$$

which is equivalent to

$$(P1.3.4): \max_{\gamma} \gamma - \frac{\rho}{2} \sum_{k=1}^K \left(\eta_k^{(j+1)} - \gamma + \eta_{d,k}^{(j)} \right)^2. \quad (30)$$

Apparently, (P1.3.4) is a concave quadratic unconstrained maximization problem, which can be readily solved by letting the first-order derivative of the objective function w.r.t. γ be zero. Then, $\gamma^{(j+1)}$ is given by

$$\gamma^{(j+1)} = \frac{\sum_{k=1}^K \left(\eta_k^{(j+1)} + \eta_{d,k}^{(j)} \right) \rho + 1}{\rho K}. \quad (31)$$

STEP 5: Updating $\{z_{d,km}^{(j+1)}, \eta_{d,k}^{(j+1)}\}$:

$\{z_{d,km}, \eta_{d,k}\}$ can be updated by

$$z_{d,km}^{(j+1)} = z_{km}^{(j+1)} - \mathbf{h}_{\text{SIM-}k}^H \mathbf{G}^{(j+1)} \mathbf{w}_{1,m} \rho_m^{(j+1)} + z_{d,km}^{(j)}, \quad (32)$$

$$\eta_{d,k}^{(j+1)} = \eta_k^{(j+1)} - \gamma^{(j+1)} + \eta_{d,k}^{(j)}. \quad (33)$$

B. Convergence and Computational Complexity Analysis

To elaborate, the proposed algorithm is summarized in Algorithm 1. The convergence behavior of the inner consensus-ADMM under similar problem structures has been consistently observed and verified in [32]–[35]. Moreover, based on (10), the outer iteration always satisfies [36]

$$\begin{aligned} r_k(\{\rho_k^{(i+1)}, \Theta_l^{(i+1)}\}) &\geq \hat{r}_{k,i}(\{\rho_k^{(i+1)}, \Theta_l^{(i+1)}\} | \{\rho_k^{(i)}, \Theta_l^{(i)}\}) \\ &\geq \hat{r}_{k,i}(\{\rho_k^{(i)}, \Theta_l^{(i)}\} | \{\rho_k^{(i)}, \Theta_l^{(i)}\}) = r_k(\{\rho_k^{(i+1)}, \Theta_l^{(i+1)}\}). \end{aligned} \quad (34)$$

Therefore, the algorithm typically converges to at least a locally optimal solution of (P1).

In general, we usually simplify the expression of computational complexity by omitting the lower order terms and constant coefficients [37]. Note that Algorithm 1 is computationally efficient, since all optimized variables are updated by closed-form expressions or the simple bisection search. By (10), (11), (12), and (13), the computational complexity of step 3 in Algorithm 1 is mainly dominated by computing $\mathbf{h}_{\text{SIM-}k}^H \mathbf{G} \mathbf{w}_{1,m} \rho_m$, for $k, m \in \mathcal{K}$, of which the computational

Algorithm 1 The proposed algorithm for MR maximization

- 1: Initialize outer iteration index i , inner consensus-ADMM iteration index j , $\rho_k^{(0)}$, $\Theta_l^{(0)}$, $\gamma^{(0)}$, $z_{d,km}^{(0)} = 0$, and $\eta_{d,k}^{(0)} = 0$, for $l \in \mathcal{L}$ and $k, m \in \mathcal{K}$.
 - 2: **repeat**
 - 3: Compute $\{\mathbf{B}_k^{(i)}\}$, $\{c_k^{(i)}\}$, and $\gamma^{(i)}$ by $\{\rho_k^{(i)}\}$ and $\{\Theta_l^{(i)}\}$.
 - 4: Set $\gamma^{(j)} = \gamma^{(i)}$, $\rho_k^{(j)} = \rho_k^{(i)}$, $\Theta_l^{(j)} = \Theta_l^{(i)}$.
 - 5: **repeat**
 - 6: Update $\{z_{d,km}^{(j+1)}\}$ and $\{\eta_k^{(j+1)}\}$ by Table II.
 - 7: Update $\{\rho_k^{(j+1)}\}$ by (24).
 - 8: Update $\{\Theta_l^{(j+1)}\}$ by (28).
 - 9: Update $\gamma^{(j+1)}$ by (31).
 - 10: Update $\{z_{d,km}^{(j+1)}, \eta_{d,k}^{(j+1)}\}$ by (32) and (33).
 - 11: $j \leftarrow j + 1$.
 - 12: **until** The growth of $\min(\{\eta_k\})$ is less than the set threshold $\zeta_{inn} > 0$, i.e., $(\min(\{\eta_k^{(j)}\}) - \min(\{\eta_k^{(j-1)}\}))/\min(\{\eta_k^{(j)}\}) \leq \zeta_{inn}$ or the maximum number of iterations $\tau_{inn} > 0$ has been reached.
 - 13: Output $\rho_k^{(i+1)} = \rho_k^{(j)}$ and $\Theta_l^{(i+1)} = \Theta_l^{(j)}$.
 - 14: $i \leftarrow i + 1$.
 - 15: **until** The growth of γ is less than the set threshold $\zeta_{out} > 0$, i.e., $(\gamma^{(i)} - \gamma^{(i-1)})/\gamma^{(i)} \leq \zeta_{out}$ or the maximum number of iterations $\tau_{out} > 0$ has been reached.
-

complexity is $\mathcal{O}(K^2 N^2)$. Similarly, the computational complexity of step 6 is $\mathcal{O}((K^2 N^2) \log_2(1/\varepsilon))$, where ε stands for the accuracy of bisection searching. Since $\mathbf{h}_{\text{SIM-}k}^H \mathbf{G}^{(j)} \mathbf{w}_{1,m}$, for $k, m \in \mathcal{K}$ has been computed in step 6, the computational complexity of step 7 is $\mathcal{O}(K^2 \log_2(1/\varepsilon))$. Likewise, the computational complexity of step 8, 9, and 10 are $\mathcal{O}(LN^3 K^2)$, $\mathcal{O}(K)$, and $\mathcal{O}(K^2 N^2)$, respectively. Finally, the overall computational complexity of Algorithm 1 can be expressed as $\mathcal{O}(I_{out}(I_{inn}((K^2 N^2) \log_2(1/\varepsilon) + K^2 \log_2(1/\varepsilon) + LN^3 K^2 + K^2 N^2) + K^2 N^2))$, where I_{inn} and I_{out} denote the numbers of iterations required for inner consensus-ADMM iteration and outer iteration, respectively.

IV. SOLVING ALGORITHM FOR GMR MAXIMIZATION

A. GMR Maximization Algorithm Design

Again, assuming $\{\rho_k^{(i)}\}$ and $\{\Theta_l^{(i)}\}$ are feasible solutions outputted in the i -th round of iteration, we can then obtain the corresponding $\{r_k^{(i)}\}$. As shown in [28], [38]–[41], for the given $\{\rho_k^{(i)}\}$ and $\{\Theta_l^{(i)}\}$, the linearized function of (8) can be expressed as

$$\xi^{(i)}(\{\rho_k, \Theta_l\}) = \sum_{k=1}^K \nabla f_{GM,k}^{(i)} r_k + \frac{K-1}{K} f_{GM}(\{r_k^{(i)}\}), \quad (35)$$

in which $f_{GM}(\{r_k^{(i)}\}) \triangleq \left(\prod_{k=1}^K r_k^{(i)}\right)^{1/K}$ and $\nabla f_{GM,k}^{(i)} = f_{GM}(\{r_k^{(i)}\})/K r_k^{(i)} \geq 0$ represents the gradient of

$f_{GM}(\{r_k\})$ w.r.t $\{r_k\}$ at feasible solution $\{r_k^{(i)}\}$. Therefore, at the i -th round, we can seek $\{\rho_k^{(i+1)}\}$ and $\{\Theta_l^{(i+1)}\}$ by solving

$$(P2.1) : \max_{\{\rho_k, \Theta_l\}} \xi^{(i)}(\{\rho_k, \Theta_l\}) \quad (36)$$

$$\text{s.t.} \quad (7b), (7c), (7d). \quad (36a)$$

Unfortunately, (P2.1) can still not be directly addressed due to the complex coupling. With the assistance of (10), (P2.1) can be transformed into two sub-problems relative to $\{\rho_k\}$ and $\{\Theta_l\}$, respectively, and then we can update both sub-problems alternately. Next, we will show the details of the alternative iteration procedure.

STEP 1: Updating $\{\rho_k^{(i+1)}\}$:

Given $\{\Theta_l^{(i)}\}$, $\{\rho_k\}$ can be updated by solving

$$(P2.1.1): \{\rho_k^{(i+1)}\} = \arg \max_{\{\rho_k\}} \sum_{k=1}^K \frac{\nabla f_{GM,k}^{(i)}}{\ln 2} \left(c_k^{(i)} - 2\Re(b_{k,12}^{(i)} \mathbf{h}_{\text{SIM-}k}^H \mathbf{G}^{(i)} \mathbf{w}_{1,k}^1 \rho_k) - b_{k,22}^{(i)} \sum_{m=1}^K |\mathbf{h}_{\text{SIM-}k}^H \mathbf{G}^{(i)} \mathbf{w}_m^1 \rho_m|^2 \right) \quad (37)$$

$$\text{s.t.} \quad (7b), (7c). \quad (37a)$$

Ignoring the non-negative constraint (7c), (P2.1.1) also becomes a convex QCQP-1 that can be solved in closed-form by multiplier method. Then, $\rho_k^{(i+1)}$ can be given by

$$\rho_k^{(i+1)} = \begin{cases} f_{k,\mu}(0), & \text{if } \sum_{k=1}^K (f_{k,\mu}(0))^2 \leq P_{\max}, \\ f_{k,\mu}(\hat{\mu}), & \text{otherwise.} \end{cases} \quad (38)$$

where

$$f_{k,\mu}(\mu) = \frac{-\nabla f_{GM,k}^{(i)} \Re(b_{k,12}^{(i)} \mathbf{h}_{\text{SIM-}k}^H \mathbf{G}^{(i)} \mathbf{w}_{1,k}^1)}{\sum_{m=1}^K \nabla f_{GM,m}^{(i)} b_{m,22}^{(i)} |\mathbf{h}_{\text{SIM-}m}^H \mathbf{G}^{(i)} \mathbf{w}_{1,k}^1|^2 + \ln 2\mu},$$

for $\mu \geq 0$, where $\hat{\mu} > 0$ is the optimal dual variable when $\sum_{k=1}^K (f_{k,\mu}(0))^2 > P_{\max}$. By substituting (12) and (13) into (38), we can see that $\{\rho_k^{(i+1)}\}$ is always non-negative. This also implies that constraint (7c) is always satisfied.

STEP 2: Updating $\{\Theta_l^{(i+1)}\}$:

Given $\{\rho_k^{(i+1)}\}$, $\{\Theta_l\}$ can be updated by solving

$$(P2.1.2): \{\Theta_l^{(i+1)}\} = \arg \max_{\{\Theta_l\}} \sum_{k=1}^K \frac{\nabla f_{GM,k}^{(i)}}{\ln 2} \left(c_k^{(i)} - 2\Re(b_{k,12}^{(i)} \mathbf{h}_{\text{SIM-}k}^H \mathbf{G} \mathbf{w}_k^1 \rho_k^{(i+1)}) - b_{k,22}^{(i)} \sum_{m=1}^K |\mathbf{h}_{\text{SIM-}k}^H \mathbf{G} \mathbf{w}_m^1 \rho_m^{(i+1)}|^2 \right) \quad (39)$$

$$\text{s.t.} \quad 0 \leq \theta_{l,n} \leq 2\pi. \quad (39a)$$

Similar to (P1.3.3), the phase shift of the n -th meta-atom on the l -th metasurface layer $\theta_{l,n}$ can be updated by solving

$$(P2.1.2_{l,n}) : \max_{\theta_{l,n}} -2\Re(q_{l,n}^{(i)} e^{j\theta_{l,n}}) \quad (40)$$

$$\text{s.t.} \quad 0 \leq \theta_{l,n} \leq 2\pi. \quad (40a)$$

Algorithm 2 The proposed algorithm for GMR maximization

-
- 1: Initialize iteration index $i = 0$, $\rho_k^{(0)}$, and $\Theta_l^{(0)}$
 - 2: **repeat**
 - 3: Compute $\{\mathbf{B}_k^{(i)}\}$ and $\{c_k^{(i)}\}$ by $\{\rho_k^{(i)}\}$ and $\{\Theta_l^{(i)}\}$.
 - 4: Given $\{\Theta_l^{(i)}\}$, update $\{\rho_k^{(i+1)}\}$ by (38).
 - 5: Given $\{\rho_k^{(i+1)}\}$, update $\{\Theta_l^{(i+1)}\}$ by (41).
 - 6: $i \leftarrow i + 1$.
 - 7: **until** The growth of $f_{GM}(\{r_k\})$ is less than the set threshold $\zeta_{GM} > 0$ or the maximum number of iterations has been reached.
-

where

$$\begin{aligned}
 q_{l,n}^{(i)} &= \left[\sum_{k=1}^K \mathbf{q}_{1,l,k}^{(i)} \right]_n - \sum_{n' \neq n}^N e^{-j\theta_{l,n'}} \left[\sum_{k=1}^K \sum_{m=1}^K \mathbf{Q}_{2,l,k,m}^{(j)} \right]_{n',n}^{(i)}, \\
 \mathbf{q}_{1,l,k}^{(i)} &= \left(\nabla f_{GM,k}^{(i)} b_{k,12}^{(i)} \mathbf{h}_{\text{SIM-}k}^H \mathbf{U}_l^{(i)} \right) \odot \left(\mathbf{V}_l^{(i)} \mathbf{w}_{1,k} \rho_k^{(i+1)} \right)^T, \\
 \mathbf{Q}_{2,l,k,m}^{(i)} &= \nabla f_{GM,k}^{(i)} b_{k,22}^{(i)} \left(\mathbf{q}_{2,l,k,m}^{(i)} \left(\mathbf{q}_{2,l,k,m}^{(i)} \right)^H \right)^T, \\
 \mathbf{q}_{2,l,k,m}^{(i)} &= \text{diag} \left(\mathbf{h}_{\text{SIM-}k}^H \mathbf{U}_l^{(i)} \right) \mathbf{V}_l^{(i)} \mathbf{w}_{1,m} \rho_m^{(i+1)}.
 \end{aligned}$$

Consequently, the optimal $\theta_{l,n}^{(i+1)}$ for (P2.1.2 $_{l,n}$) is given by

$$\theta_{l,n}^{(i+1)} = \pi - \arg \left(q_{l,n}^{(i)} \right). \quad (41)$$

Algorithm 2 provides the pseudo-code for the proposed steepest descent procedure to solve (P2.1). The iterations of (38) and (41) obtain a descent direction by finding a better feasible point for the non-convex problem (P2). This surrogate-based strategy is similar to the Frank-and-Wolfe method [38], which guarantees convergence to a stationary point under mild conditions. According to [38], [41], [42], by repeatedly alternating the iterations of (38) and (41), the algorithm typically converges to at least a locally optimal solution of (P2). The overall computational complexity of Algorithm 2 can be expressed as $\mathcal{O}(I_{GM}((K^2 N^2)(\log_2(1/\epsilon) + 1) + LN^3 K^2))$, where I_{GM} denotes the numbers of iterations required for convergence.

B. Solving Algorithm for SR Maximization

By (P2.1), we can observe that both $\nabla f_{GM,k}^{(i)}$ and $f_{GM}(\{r_k^{(i)}\})$ are constant terms in the i -th iteration, because both of which are determined by $\{r_k^{(i)}\}$, not $\{r_k\}$. Therefore, if we let $\nabla f_{GM,k}^{(i)} = 1$ and $f_{GM}(\{r_k^{(i)}\}) = 0$ in each iteration, the optimization objective in (P2.1) becomes $\sum_{k=1}^K r_k$, representing the system SR. Then, Algorithm 2 can be directly applied to the SR maximization.

Remark 1. For the three problems of MR maximization, GMR maximization, and SR maximization, we have derived the corresponding closed-form solutions. Notably, the algorithmic complexity decreases progressively from MR to GMR and then to SR. MR maximization is appropriate for scenarios where user fairness is a primary consideration, as it aims to improve the performance of the user with the lowest

TABLE III
SIMULATION PARAMETERS

Parameter	Value
K, M	4, 4
P_{\max}	20 dBm
σ_k^2	-96 dBm
λ_c	0.0107m (28 GHz) [10]
$\alpha_{\text{SIM-}k}$	3
$G_{\text{BS}}, G_k, \forall k$	5 dBi, 0 dBi [43]
ρ	100
$\zeta_{\text{inn}}, \zeta_{\text{out}}, \zeta_{GM}$	$10^{-4}, 10^{-5}, 10^{-5}$
$\tau_{\text{inn}}, \tau_{\text{out}}, \tau_{GM}$	5000, 8000, 8000
d_l, d_w, d_t	$0.5\lambda_c, 0.5\lambda_c, 5\lambda_c$ [11], [13]

rate. GMR maximization offers a balanced trade-off between fairness and throughput, making it suitable for environments with moderate user heterogeneity. SR maximization focuses on maximizing the overall system throughput and is generally more effective when all users experience the same degree of large-scale fading.

V. NUMERICAL EVALUATION

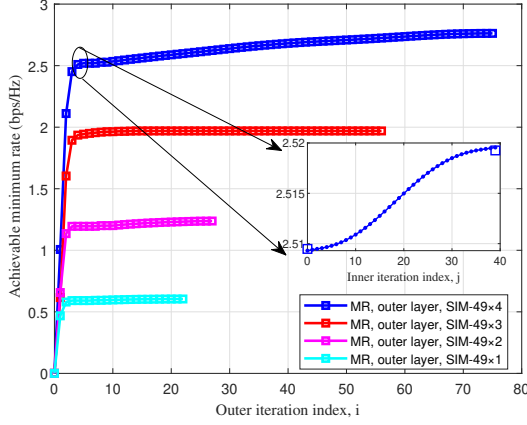
A. Evaluation Scenarios and Parameters

We consider a 3-dimension (x-y-z coordinate system) simulation environment and the unit of distance is 1 meter. Specifically, the BS is equipped with a uniform linear array (ULA) with few antennas and each layer of the SIM arrangement is identically equipped with a uniform planar array (UPA) containing $N = N_x N_z$ elements, where N_x and N_z are the numbers of elements along x-axis and z-axis, respectively. Next we assume that $N_x = N_z$. Importantly, the BS transmit antennas along z-axis are integrated with the SIM to facilitate beamforming design in the EM wave domain [10]. The SIM is deployed on the x-z plane with the reference meta-atom located at (0, 0, 0), and all K users are randomly distributed in the user cluster centered at (0, 60, 0) with radius 50m.

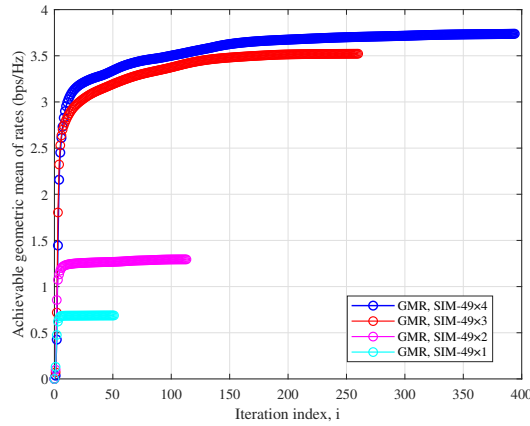
For the channel from the SIM to the k -th user, path loss coefficient is equal to $\beta_{\text{SIM-}k} = 10^{(G_{\text{BS}} + G_k - 33.05)/10} d_{\text{SIM-}k}^{-\alpha_{\text{SIM-}k}}$, where G_{BS} and G_k represent the antenna gains of BS and user k , respectively, $d_{\text{SIM-}k}$ represents the link distance from the SIM to the k -th user, and $\alpha_{\text{SIM-}k}$ represents the path loss exponent. Denote the spatial correlation matrix of the SIM w.r.t. the k -th user by $\mathbf{R}_{\text{SIM-}k} \in \mathbb{C}^{N \times N}$ and there is $[\mathbf{R}_{\text{SIM-}k}]_{n,n'} = e^{j\pi(n-n') \sin \psi_k \sin \varphi_k}$ in which ψ_k and φ_k are the azimuth and elevation angle w.r.t. user k , respectively. Assume the channel from the SIM to each user experience Rayleigh fading, then we have $\mathbf{h}_{\text{SIM-}k}^H \sim \mathcal{CN}(0, \beta_{\text{SIM-}k} \mathbf{R}_{\text{SIM-}k})$. Unless otherwise stated later, Table III demonstrates all the parameter settings. In the following legend, SIM- $N \times L$ means the SIM has L layers of metasurfaces and there are N meta-atoms on each layer.

B. Convergence of the Proposed Algorithms

Fig. 2 illustrates the convergence behavior of the proposed optimization algorithms. Both Algorithm 1 and Algorithm 2 consistently converge to stable solutions under various parameter settings, demonstrating the robustness and effectiveness



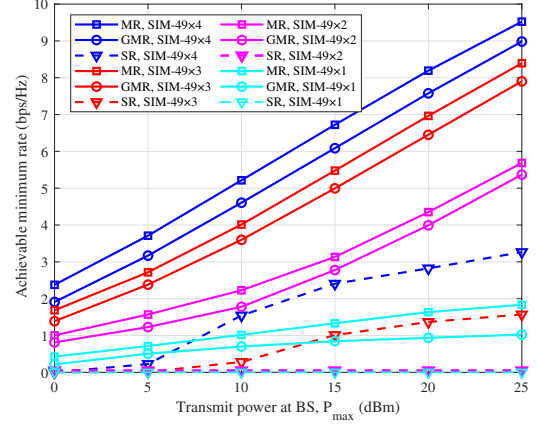
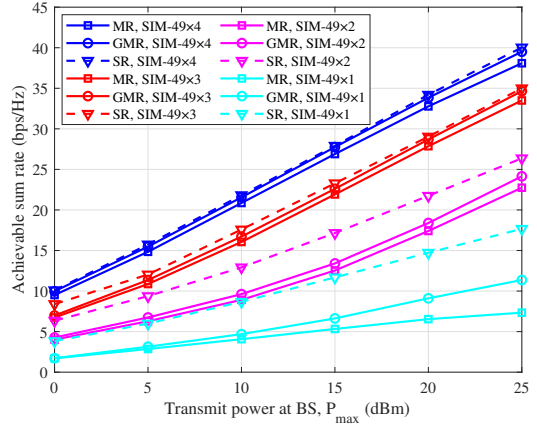
(a) Convergence behavior of Algorithm 1.



(b) Convergence behavior of Algorithm 2.

Fig. 2. Convergence behavior with $M = K = 6$ and $P_{\max} = 10\text{dBm}$.

of the proposed framework. Specifically, Fig. 2(a) presents the overall convergence process of Algorithm 1. In this figure, the horizontal axis corresponds to the outer iteration index, while the vertical axis indicates the minimum user rate. The results clearly confirm the stability and monotonic improvement of the outer-loop iterations, i.e., (34). To provide further insight, we zoom in on the MR performance of the SIM-49 \times 4 configuration between the 4th and 5th outer iterations. As shown, the convergence trajectory of the inner consensus-ADMM subproblem can be clearly observed, verifying the efficiency of the inner-layer updates in achieving accurate solutions within a few iterations. Fig. 2(b) illustrates the convergence process of Algorithm 2, where a similar pattern of rapid and stable convergence is observed. Unlike Algorithm 1, Algorithm 2 adopts a single-layer iterative approach, resulting in a smoother convergence trajectory. In addition, as the number of SIM layers increases, the feasible space of the optimization variables expands, requiring more iterations to achieve convergence. Nevertheless, increasing the number of SIM layers also leads to improved MR and GMR performance, due to the higher DoF available for approximating the desirable beamforming matrix.

Fig. 3. Achievable MR versus the maximum allowable transmit power P_{\max} .Fig. 4. Achievable SR versus the maximum allowable transmit power P_{\max} .

C. Rate Fairness Performance Comparisons

Fig. 3 depicts the achievable MR versus the maximum allowable transmit power P_{\max} . With the same parameter setting, MR maximization always achieves the highest MR, whereas SR maximization yields the worst performance, even zero rate when $L = 1, 2$. Also, we can see that increasing the number of SIM layers enhances the MR. However, it is important to note that the increase in MR when the number of SIM layers L rises from 1 to 2 is more significant than the gain observed when increasing L from 2 to 3. It indicates that increasing L can enhance the MR, but diminishing return exists. Fig. 4 presents achievable SR versus P_{\max} . In contrast to Fig. 3, SR maximization achieves the best performance, while MR maximization performs the worst. Therefore, in both scenarios, we see that GMR maximization offers a more balanced rate performance than MR maximization and SR maximization, effectively representing the trade-off of rate fairness and overall rate performance.

In Table IV, we present the rate standard deviations of all users through three rate optimization algorithms. Note that, to avoid statistical fluctuation, referring to the range of user rates, we herein approximately deem the rate standard deviation as zero if it is less than 10^{-3} bps/Hz. With the same P_{\max} , MR

TABLE IV
RATE STANDARD DEVIATIONS OF USERS

P_{\max} Schemes	0dBm	5dBm	10dBm	15dBm	20dBm
MR, SIM-49×4	0	0	0	0	0
GMR, SIM-49×4	0.48	0.58	0.64	0.69	0.72
SR, SIM-49×4	2.43	2.81	3.06	3.29	3.67
MR, SIM-49×3	0	0	0	0	0
GMR, SIM-49×3	0.38	0.50	0.58	0.67	0.72
SR, SIM-49×3	2.33	2.62	2.95	3.46	4.07
MR, SIM-49×2	0	0	0	0	0
GMR, SIM-49×2	0.37	0.55	0.67	0.76	0.78
SR, SIM-49×2	2.02	2.64	2.89	3.46	4.20
MR, SIM-49×1	0	0	0	0	0
GMR, SIM-49×1	0.28	0.35	0.54	0.89	1.48
SR, SIM-49×1	1.71	2.04	2.63	3.47	4.29

TABLE V
THE RATIO OF THE MINIMUM RATE TO THE MAXIMUM RATE

P_{\max} Schemes	0dBm	5dBm	10dBm	15dBm	20dBm
MR, SIM-49×4	0.9998	0.9999	0.9999	0.9999	0.9999
GMR, SIM-49×4	0.6445	0.7099	0.7623	0.7981	0.8215
SR, SIM-49×4	0	0.0210	0.1755	0.2928	0.3653
MR, SIM-49×3	0.9999	0.9999	0.9999	0.9999	0.9999
GMR, SIM-49×3	0.6238	0.6851	0.7358	0.7718	0.7978
SR, SIM-49×3	0	0.0022	0.0590	0.1358	0.1755
MR, SIM-49×2	0.9998	0.9999	0.9999	0.9999	0.9999
GMR, SIM-49×2	0.5236	0.5153	0.5500	0.6262	0.6998
SR, SIM-49×2	0	0	0	0	0
MR, SIM-49×1	0.9997	0.9998	0.9998	0.9998	0.9998
GMR, SIM-49×1	0.2693	0.2567	0.3306	0.3902	0.4017
SR, SIM-49×1	0	0	0	0	0

maximization nearly has zero deviation, followed by GMR maximization, and SR maximization achieves the largest standard deviation. It indicates that MR maximization is the fairest solution and SR maximization has the least fairness. As P_{\max} increases, the rate standard deviations of MR maximization remains zero, indicating the minimum rate variation. GMR maximization shows a slight increase in standard deviation but stays at a very low level. In contrast, SR maximization exhibits greater fluctuations, with standard deviations ranging from 1.71 to 4.29, reflecting a less stable rate distribution.

Table V illustrates the ratio of the minimum rate to the maximum rate versus P_{\max} . This ratio, ranging from 0 to 1, quantifies rate fairness, with 1 indicating perfect fairness and lower values reflecting increased disparity. Simulation results demonstrate that MR maximization and GMR maximization achieve far higher ratios than SR maximization, underscoring their superiority in fairness enhancement. As P_{\max} increases, the ratio for MR maximization remains near 1 across different SIM layer configurations, demonstrating its robustness in maintaining fairness. However, some ratios for SR maximization is zero, which indicates the inability to attain a satisfactory rate.

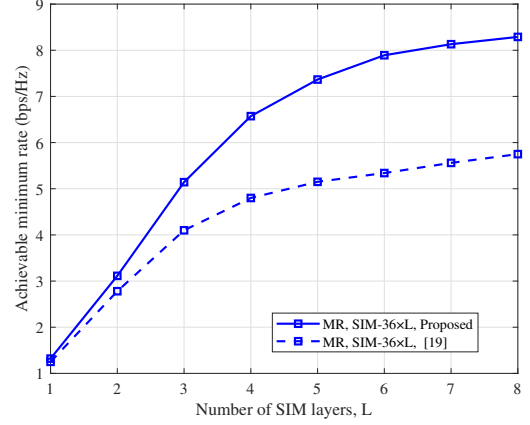


Fig. 5. MR comparison of the proposed Algorithm 1 and [19] with same parameters setups as in [19].

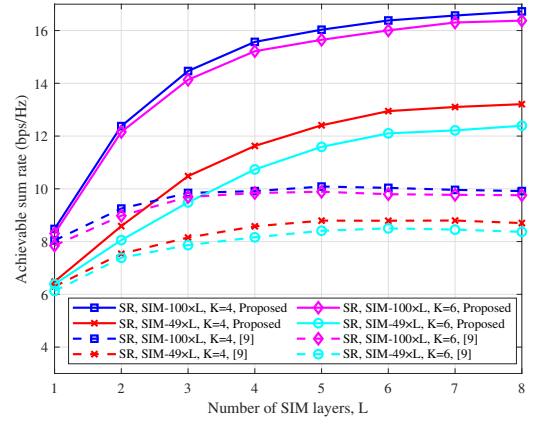


Fig. 6. SR comparison of the proposed Algorithm 2 and [9] with same parameters setups as in [9].

D. Performance Comparison with Existing Works

To further evaluate the effectiveness of the proposed Algorithm 1, we compare its MR performance with [19] in Fig. 5¹. For a fair comparison, we adopt the same parameters setups as in [19]. The superior performance of Algorithm 1 primarily arises from two factors. First, while [19] typically focus on MSINR maximization, our approach directly optimizes the MR metric, which better captures user fairness at the rate level. Second, we derive a closed-form solution for the SIM phase shifts, eliminating the dependence on iterative gradient descent methods and thereby enhancing solution accuracy. It can be observed that as L increases, the performance gap between the proposed algorithm and [19] becomes increasingly significant, which further validates the second reason discussed above. Similarly, to assess the performance of the proposed Algorithm 2 for SR maximization, Fig. 6 presents a comparison between Algorithm 2 and [9]. Since most existing studies on SR maximization generally employ water-filling or gradient descent-based methods, we adopt the widely recognized classical work

¹The code of the proposed algorithms for MR and SR maximization are available at: <https://github.com/JunjieFangXJTU/Proposed>

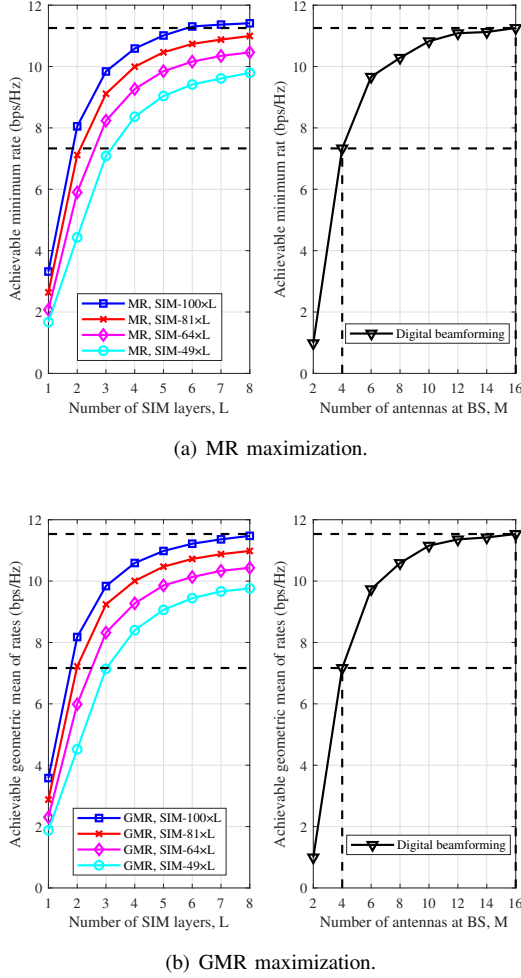


Fig. 7. Comparison of SIM beamforming and digital beamforming.

[9] as the benchmark². For a fair comparison, we here also set the identical configuration parameters as in [9]. As L increases, the proposed algorithm demonstrates gradually increasing SR gains, e.g., outperforming the benchmark algorithm by 35.36% at SIM-100 \times 2, 66.65% at SIM-100 \times 6, and 67.83% at SIM-100 \times 8 for $K = 6$.

E. Rate Comparison With Digital Beamforming

Fig. 7 compares the user rate performance of the proposed SIM beamforming schemes (the left subplot) and digital beamforming (DB) scheme without SIM (the right subplot) in multiuser MISO downlink systems, using MR and GMR as performance metrics, respectively. Notably, in the considered schemes, the BS is equipped with only 4 transmit antennas (i.e., 4 RF chains). In contrast, for the DB scheme, the number of antennas M is equal to the number of the required RF chains. For DB for MR maximization and GMR maximization, we adopt the algorithms from [33] and [38], respectively. Firstly, in SIM beamforming scheme, we can see that increasing L or N enhances rate performance. While in DB

scheme, increasing the number of transmit antennas can also enhance the rate performance. DB reaches its performance limit at $M = 16$, whereas the SIM beamforming schemes approach their rate limits at $L = 8$ under different meta-atom configurations. Since the proposed schemes solely rely on power allocation without phase adjustment at BS, DB with $M = 4$ outperforms SIM beamforming with $L = 1$. However, SIM beamforming with $L = 2$ and $N = 100$ surpasses DB at $M = 4$, and all SIM beamforming schemes with $L = 3$ outperform DB with $M = 4$. Interestingly, SIM beamforming with $L = 6$ and $N = 100$ achieves a similar rate as DB with $M = 16$, which reveals that we can adopt SIM to replace multiple antennas in terms of rate performance, as suggested in [9]–[12]. For a fair comparison, we also evaluate the power consumption of both beamforming schemes. The total power consumption is given by $P_{tol} = P_{max} + MP_{RF} + P_0 + LNP_{SIM}$, where $P_{RF} = 30$ dBm is the circuit power consumption of each RF chain, $P_0 = 40$ dBm is the BS base power consumption, and $P_{SIM} = 10$ dBm is the power consumption per SIM meta-atom [44]. Assuming P_0 is the same for all schemes, SIM beamforming with 100 \times 6 consumes 20.1W, lower than the power 26.1W required by DB at $M = 16$.

VI. CONCLUSION

In this paper, we investigated rate fairness optimization for SIM-assisted multiuser systems through two optimization problems: MR maximization and GMR maximization. We gave two low-complexity algorithms based on closed-form solutions, respectively. Numerical results confirmed the benefits of SIM deployment and validated the convergence of the proposed algorithms. It also reveals: 1) MR maximization ensures near-perfect fairness and GMR maximization achieves a balance between fairness and SR; 2) For MR and SR, the proposed algorithms remarkably outperforms the benchmark algorithms; 3) SIM beamforming can achieve comparable performance to DB while consuming less power.

REFERENCES

- [1] C. Wang, X. You, X. Gao *et al.*, “On the Road to 6G: Visions, Requirements, Key Technologies, and Testbeds,” *IEEE Communications Surveys & Tutorials*, vol. 25, no. 2, pp. 905–974, 2023.
- [2] Q. Wu, B. Zheng, C. You *et al.*, “Intelligent Surfaces Empowered Wireless Network: Recent Advances and the Road to 6G,” *Proc. IEEE*, vol. 112, no. 7, pp. 724–763, Jul. 2024.
- [3] Q. Wu, S. Zhang, B. Zheng *et al.*, “Intelligent Reflecting Surface-Aided Wireless Communications: A Tutorial,” *IEEE Trans. Commun.*, vol. 69, no. 5, pp. 3313–3351, May 2021.
- [4] C. Huang, S. Hu, G. C. Alexandropoulos *et al.*, “Holographic MIMO Surfaces for 6G Wireless Networks: Opportunities, Challenges, and Trends,” *IEEE Wirel. Commun.*, vol. 27, no. 5, pp. 118–125, Oct. 2020.
- [5] Q. Wu, T. Q. Duong, D. Wing Kwan Ng *et al.*, *Intelligent Surfaces Empowered 6G Wireless Network*. John Wiley & Sons, 2023.
- [6] L. Wei, C. Huang, G. C. Alexandropoulos *et al.*, “Multi-User Holographic MIMO Surfaces: Channel Modeling and Spectral Efficiency Analysis,” *IEEE J. Sel. Topics Signal Process.*, vol. 16, no. 5, pp. 1112–1124, Aug. 2022.
- [7] Q. Wu and R. Zhang, “Intelligent Reflecting Surface Enhanced Wireless Network via Joint Active and Passive Beamforming,” *IEEE Trans. Wireless Commun.*, vol. 18, no. 11, pp. 5394–5409, Nov. 2019.
- [8] C. Liu, Q. Ma, Z. J. Luo *et al.*, “A programmable diffractive deep neural network based on a digital-coding metasurface array,” *Nature Electronics*, vol. 5, no. 2, pp. 113–122, Feb. 2022.

²The code of [9] is sourced from: <https://github.com/JianchengAn/SIM-2-MUMISO>

- [9] J. An, M. Di Renzo, M. Debbah *et al.*, “Stacked Intelligent Metasurfaces for Multiuser Beamforming in the Wave Domain,” in *ICC 2023 - IEEE International Conference on Communications*, 2023, pp. 2834–2839.
- [10] J. An, C. Xu, D. W. K. Ng *et al.*, “Stacked Intelligent Metasurfaces for Efficient Holographic MIMO Communications in 6G,” *IEEE J. Sel. Areas Commun.*, vol. 41, no. 8, pp. 2380–2396, Aug. 2023.
- [11] J. An, C. Yuen, C. Xu *et al.*, “Stacked Intelligent Metasurface-Aided MIMO Transceiver Design,” *IEEE Wirel. Commun.*, vol. 31, no. 4, pp. 123–131, Aug. 2024.
- [12] J. An, C. Yuen, Y. L. Guan *et al.*, “Two-Dimensional Direction-of-Arrival Estimation Using Stacked Intelligent Metasurfaces,” *IEEE J. Sel. Areas Commun.*, vol. 42, no. 10, pp. 2786–2802, Oct. 2024.
- [13] J. An, M. D. Renzo, M. Debbah *et al.*, “Stacked Intelligent Metasurfaces for Multiuser Downlink Beamforming in the Wave Domain,” *IEEE Trans. Wireless Commun.*, pp. 1–1, 2025.
- [14] A. Papazafeiropoulos, P. Kourtessis, S. Chatzinotas *et al.*, “Achievable Rate Optimization for Large Stacked Intelligent Metasurfaces Based on Statistical CSI,” *IEEE Wireless Commun. Lett.*, vol. 13, no. 9, pp. 2337–2341, Sep. 2024.
- [15] S. Lin, J. An, L. Gan *et al.*, “Stacked Intelligent Metasurface Enabled LEO Satellite Communications Relying on Statistical CSI,” *IEEE Wireless Commun. Lett.*, vol. 13, no. 5, pp. 1295–1299, May 2024.
- [16] H. Liu, J. An, G. C. Alexandropoulos *et al.*, “Multi-User MISO with Stacked Intelligent Metasurfaces: A DRL-Based Sum-Rate Optimization Approach,” *IEEE Trans. on Cogn. Commun. Netw.*, pp. 1–1, 2025.
- [17] M. R. Kavianinia, A. Mohammadi, and V. Meghdadi, “Secrecy Rate Maximization in the Presence of Stacked Intelligent Metasurface,” *IEEE Trans. Inf. Forensics Secur.*, pp. 1–1, 2025.
- [18] S. Li, F. Zhang, T. Mao *et al.*, “Transmit Beamforming Design for ISAC With Stacked Intelligent Metasurfaces,” *IEEE Trans. Veh. Technol.*, vol. 74, no. 4, pp. 6767–6772, Apr. 2025.
- [19] N. Ginige, P. Dharmawansa, A. S. de Sena *et al.*, “Max-Min Fairness for Stacked Intelligent Metasurface-Assisted Multi-User MISO Systems,” *IEEE Open Journal of the Communications Society*, pp. 1–1, 2025.
- [20] Y. Sun, K. An, M. Yu *et al.*, “Dual-Polarized Stacked Metasurface Transceiver Design With Rate Splitting for Next-Generation Wireless Networks,” *IEEE J. Sel. Areas Commun.*, vol. 43, no. 3, pp. 811–833, Mar. 2025.
- [21] A. Papazafeiropoulos, P. Kourtessis, S. Chatzinotas *et al.*, “Performance of Double-Stacked Intelligent Metasurface-Assisted Multiuser Massive MIMO Communications in the Wave Domain,” *IEEE Trans. Wireless Commun.*, vol. 24, no. 5, pp. 4205–4218, May 2025.
- [22] Y. Hu, J. Zhang, E. Shi *et al.*, “Joint Beamforming and Power Allocation Design for Stacked Intelligent Metasurfaces-Aided Cell-Free Massive MIMO Systems,” *IEEE Trans. Veh. Technol.*, vol. 74, no. 3, pp. 5235–5240, Mar. 2025.
- [23] Q. Li, M. El-Hajjar, C. Xu *et al.*, “Stacked Intelligent Metasurfaces for Holographic MIMO Aided Cell-Free Networks,” *IEEE Trans. Commun.*, vol. 72, no. 11, pp. 7139–7151, Nov. 2024.
- [24] A. Papazafeiropoulos, J. An, P. Kourtessis *et al.*, “Achievable Rate Optimization for Stacked Intelligent Metasurface-Assisted Holographic MIMO Communications,” *IEEE Trans. Wireless Commun.*, pp. 1–1, 2024.
- [25] E. E. Bahingayi, N. S. Perović, and L.-N. Tran, “Scaling Achievable Rates in SIM-aided MIMO Systems with Metasurface Layers: A Hybrid Optimization Framework,” *IEEE Wireless Commun. Lett.*, pp. 1–1, 2025.
- [26] X. Yao, J. An, L. Gan *et al.*, “Channel Estimation for Stacked Intelligent Metasurface-Assisted Wireless Networks,” *IEEE Wireless Commun. Lett.*, vol. 13, no. 5, pp. 1349–1353, May 2024.
- [27] Q.-U.-A. Nadeem, J. An, and A. Chaaban, “Hybrid Digital-Wave Domain Channel Estimator for Stacked Intelligent Metasurface Enabled Multi-User MISO Systems,” in *2024 IEEE Wireless Communications and Networking Conference (WCNC)*, 2024, pp. 1–6.
- [28] H. Yu, H. D. Tuan, A. A. Nasir *et al.*, “Rate-Fairness-Aware Low Resolution RIS-Aided Multi-User OFDM Beamforming,” *IEEE Trans. Veh. Technol.*, vol. 73, no. 2, pp. 2401–2415, Feb. 2024.
- [29] M. M. Naghsh, M. Masjedi, A. Adibi *et al.*, “Max–Min Fairness Design for MIMO Interference Channels: A Minorization–Maximization Approach,” *IEEE Trans. Signal Process.*, vol. 67, no. 18, pp. 4707–4719, Sep. 2019.
- [30] J. Fang, C. Zhang, Q. Wu *et al.*, “Improper Gaussian Signaling for IRS Assisted Multiuser SWIPT Systems With Hardware Impairments,” *IEEE Trans. Veh. Technol.*, vol. 72, no. 10, pp. 13 024–13 038, Oct. 2023.
- [31] —, “Improper Gaussian Signaling for STAR-RIS assisted Multiuser MISO Interference Channels,” in *GLOBECOM 2023*, 2023, pp. 1399–1404.
- [32] K. Huang and N. D. Sidiropoulos, “Consensus-ADMM for General Quadratically Constrained Quadratic Programming,” *IEEE Trans. Signal Process.*, vol. 64, no. 20, pp. 5297–5310, Oct. 2016.
- [33] J. Fang, C. Zhang, Q. Wu *et al.*, “A Two-Layer Iterative Algorithm for Max-Min Rate Optimization in IRS Assisted Multiuser Systems With Improper Gaussian Signaling,” *IEEE Trans. Commun.*, vol. 72, no. 12, pp. 7596–7610, Dec. 2024.
- [34] S. Boyd, N. Parikh, E. Chu *et al.*, *Distributed Optimization and Statistical Learning via the Alternating Direction Method of Multipliers*. Now Foundations and Trends, 2011.
- [35] M. Hong and Z. Luo, “On the Linear Convergence of the Alternating Direction Method of Multipliers,” *Math. Programming*, vol. 162, p. 165–199, Mar. 2017.
- [36] H. Yu, H. D. Tuan, A. A. Nasir *et al.*, “Joint Design of Reconfigurable Intelligent Surfaces and Transmit Beamforming Under Proper and Improper Gaussian Signaling,” *IEEE J. Sel. Areas Commun.*, vol. 38, no. 11, pp. 2589–2603, Nov. 2020.
- [37] S. Boyd and L. Vandenberghe, *Convex Optimization*. Cambridge University Press, 2004.
- [38] H. Yu, H. D. Tuan, E. Dutkiewicz *et al.*, “Maximizing the Geometric Mean of User-Rates to Improve Rate-Fairness: Proper vs. Improper Gaussian Signaling,” *IEEE Trans. Wireless Commun.*, vol. 21, no. 1, pp. 295–309, Jan. 2022.
- [39] Y. Chen, H. D. Tuan, Y. Fang *et al.*, “Enhancing the Downlink Rate Fairness of Low-Resolution Active RIS-Aided Signaling by Closed-Form Expression-Based Iterative Optimization,” *IEEE Trans. Veh. Technol.*, vol. 73, no. 6, pp. 8013–8029, Jun. 2024.
- [40] H. D. Tuan, A. A. Nasir, H. Q. Ngo *et al.*, “Scalable User Rate and Energy-Efficiency Optimization in Cell-Free Massive MIMO,” *IEEE Trans. Commun.*, vol. 70, no. 9, pp. 6050–6065, Sep. 2022.
- [41] W. Zhu, H. D. Tuan, E. Dutkiewicz *et al.*, “Low-Complexity Pareto-Optimal 3D Beamforming for the Full-Dimensional Multi-User Massive MIMO Downlink,” *IEEE Trans. Veh. Technol.*, vol. 72, no. 7, pp. 8869–8885, Jul. 2023.
- [42] A. A. Nasir, H. D. Tuan, E. Dutkiewicz *et al.*, “Low-Resolution RIS-Aided Multiuser MIMO Signaling,” *IEEE Trans. Commun.*, vol. 70, no. 10, pp. 6517–6531, Oct. 2022.
- [43] Q.-U.-A. Nadeem, A. Kammoun, A. Chaaban *et al.*, “Asymptotic Max-Min SINR Analysis of Reconfigurable Intelligent Surface Assisted MISO Systems,” *IEEE Trans. Wireless Commun.*, vol. 19, no. 12, pp. 7748–7764, Dec. 2020.
- [44] N. S. Perović, E. E. Bahingayi, and L.-N. Tran, “Energy-Efficient Designs for SIM-Based Broadcast MIMO Systems,” *arXiv e-prints*, p. arXiv:2409.00628, Sep. 2024.